Metal-Capped Brownian and Magnetically Modulated Optical Nanoprobes (MOONs): Micromechanics in Chemical and Biological Microenvironments†

Caleb J. Behrend,‡,# Jeffrey N. Anker,‡,# Brandon H. McNaughton,‡ Murphy Brasuel,|| Martin A. Philbert,§ and Raoul Kopelman*,‡

Department of Chemistry and School of Public Health, University of Michigan Ann Arbor, Michigan 48109-1055, and Chemistry Department, Colorado College, Colorado Springs, Colorado 80903

Received: February 10, 2004

Modulated optical nanoprobes (MOONs) are microscopic (spherical and aspherical) fluorescent particles designed to emit varying intensities of light in a manner that depends on particle orientation. MOONs can be prepared over a broad size range, allowing them to be tailored to applications including intracellular sensors, using submicrometer MOONs, and immunoassays, using 1−10 μm MOONs. When particle orientation is controlled remotely, using magnetic fields (MagMOONs), it allows modulation of fluorescence intensity in a selected temporal pattern. In the absence of external fields, or material that responds to external fields, the particles tumble erratically due to Brownian thermal forces (Brownian MOONs). These erratic changes in orientation cause the MOONs to blink. The temporal pattern of blinking reveals information about the local rheological environment and any forces and torques acting on the MOONs, including biomechanical forces as observed in macrophages. The rotational diffusion rate of Brownian MOONs is inversely proportional to the particle volume and hydrodynamic shape factor, for constant temperature and viscosity. Changes in the particle volume and shape due to binding, deformation, or aggregation can be studied using the temporal time pattern from the probes. The small size and the large number of MOONs that can be viewed simultaneously provide local measurements of physical properties, in both homogeneous and inhomogeneous media, as well as global statistical ensemble properties.

Introduction

Most fluorescent nanospheres and microspheres emit light uniformly in all directions. By purposefully constructing fluorescent nanoparticles that emit anistropically, it becomes possible to monitor particle orientation and to modulate the light emitted from the particles as they rotate.[1−4] Tracking the orientation of these modulated optical nanoprobes (MOONs) allows one to observe torques acting on the MOONs. Analyzing these torques reveals information about the MOONs and the environment around them. By measuring the effect of these torques on particle fluorescence it becomes possible to observe and measure, on a microscopic scale, viscoelastic properties, thermal fluctuations, molecular and physical interactions, and vorticity in fluid flow.

Modulated optical signals stand out against zero-frequency background fluorescence, allowing sensitive physical and chemical optical analysis in the presence of high background signals, such as autofluorescence in biological samples.[1] MagMOONs are MOONs containing magnetic material that orient in response to external magnetic fields. The fluorescence from MagMOONs is magnetically modulated in a selectable temporal pattern. This modulation allows for improved sensitivity and reduced procedural complexity for fluorescent immunoassays and chemical measurement. When MagMOONs are used for immunoassay applications the surface of the MagMOONs is first functionalized with molecular recognition elements, to which analyte binds and is subsequently labeled, leading to a change in MagMOON fluorescence. By modulating MagMOONs, their emitted signal can be separated from the optical and electronic backgrounds, including autofluorescence and excess fluorescent dye not attached to the particle. This reduction in background interference leads to more sensitive measurements and enables homogeneous protocols with fewer procedural steps.[1,2]

In the absence of external rotating magnetic fields, the only surviving rotational motion of the nanoparticles or nanospheres is due to Brownian motion (rotation). As a result of this motion the particles blink erratically. This temporal pattern of blinking contains information about the local rheological environment and any forces and torques acting on the MOONs. MOONs are a new tool that makes it possible to study fundamental properties of soft materials, complex liquids, inhomogeneous liquids, liquid crystals, and biological environments.

Translational and rotational diffusion of molecules is studied by optical techniques such as fluorescence anisotropy, fluorescence recovery after photobleaching (FRAP), and fluorescence correlation spectroscopy.[5] To measure translational diffusion on larger size scales, from about 50 nm to 5 μm, the motion of nanospheres and microspheres are observed while they are pulled through the solution with laser tweezers,[6] magnetic tweezers,[7] or move under the influence of Brownian forces.[8] It is possible to locally measure the complex viscoelastic shear modulus as a function of modulation frequency[9] as well as bulk material properties using correlations in motions of diffusing microparticles.[10]

† Part of the special issue "Gerald Small Festschrift".

* Corresponding author. E-mail: kopelman@umich.edu.
‡ Chemistry Department, University of Michigan.
|| Chemistry Department, Colorado College.
§ School of Public Health, University of Michigan.
# These authors contributed equally to this article.

10.1021/jp040125g CCC: $27.50
Published on Web 06/29/2004

The rotational motion of microspheres and nanospheres has proven more difficult to measure. Dynamic light scattering and polarized FRAP are used to determine rotational diffusion coefficients for ensembles of particles; however, these techniques generally acquire an average over a large number of particles and are effected by scattering.[11] Particle orientation may also be determined by measuring the average magnetic moment from magnetized particles.[12,13] However, the magnetic methods provide information only on the average particle and require a relatively large number of magnetic particles to obtain an accurate reading.[14] Alternatively, particle orientation may be observed directly, but only if each particle is large enough and has an observable landmark[15−17] or is not spherical in shape.[18,19] For heterogeneous fluids the viscosity is a complex function of both the time scales involved and the size scale of the probing instrument.

Large batches of metal-capped nanoparticles can be prepared with carefully chosen sizes. A number of metal-capped and moon-shaped particle preparation processes have been described.[20−26] Recently, 300 nm to 3 μm moon-shaped particles were used to observe Brownian rotation[1] and measure viscosity.[3] Similarly, 960 nm moon-shaped particles were used to observe interactions with surfaces.[27]

Theory

Historically, the observation and theory of Brownian rotation has helped shape our views of matter. In 1828, Robert Brown observed "Brownian" rotation in relatively large aspherical pollen grains.[28,29] Einstein (1906) derived an equation for rotational diffusion (angle θ) as well as the rotational diffusion coefficient D^{rot} for a spherical particle;[30]

$$\langle \Delta\theta^2 \rangle = 2D^{rot}t \tag{1}$$

$$D^{rot} = RT/8\pi N_0 \eta r^3 \tag{2}$$

where r is the radius of the (spherical) particle, η is the viscosity, T the temperature, R the gas constant, and N_0 Avogadro's number. Jean Perrin (1909) utilized this approach to determine Avogadro's number, providing strong evidence for the molecular theory of matter.[16] Perrin's visual observations utilized particles approximately 10 μm in diameter, with recognizable defects whose rotations could be observed directly. The rotational diffusion rate can be measured in terms of root mean square degrees rotated, or by the shape of the autocorrelation function of the intensity time fluctuations, for particles undergoing Brownian rotation.[3,11,13] When θ is allowed to only rotate between 0° and 180° (periodic boundary conditions make 181° = 1°), $\langle \Delta\theta^2 \rangle$ approaches a maximum value as $1 - e^{-2Dt}$.[11]

Experiments using magnetic fields to rotate 4.4 μm magnetically modulated optical nanoprobes (MagMOONs) indicated that the fluorescence intensity is proportional to the cosine of the azimuthal angle of the particles, with weaker harmonics also appearing.[1] Assuming that the fluorescence intensity from Brownian MOONs is also proportional to the cosine of the azimuthal angle, the autocorrelation function, $G^{rot}(t)$, of the fluctuations is expected to decay exponentially (eq 3).[13]

$$G^{rot}(t) = e^{-t/\tau} \tag{3a}$$

$$\tau = \kappa V \eta / 2k_B T \tag{3b}$$

For a spherical particle, the shape factor κ is 6. For aspherical particles, the shape factor depends on the relative dimensions of the particle. The rotation time depends on the volume, V, of the particle and is proportional to the viscosity of the surrounding solvent environment. If harmonics are present in the angular intensity distribution, the autocorrelation function is expected to decay more quickly. Table 1 illustrates characteristic autocorrelation decay times calculated for several sizes of particles in solutions of different viscosity (and temperature).

TABLE 1: Calculated Rotational Correlation Time, τ_c, for 13, 4.4, 2, 1, 0.30, 0.1, and 0.05 μm Spherical Particles in Pure Water at 20 and 37 °C and 98% Glycerol Solution at 20 °C[a]

sphere diameter (μm)	water 37 °C (0.7 Pa·s)	water 20 °C (1.0 mPa·s)	98% glycerol 20 °C (957 mPa·s)
13	9.8 min	14 min	9.3 day
4.4	22 s	32 s	8.7 hr
2	2.1 s	3.1 s	48 min
1	270 ms	380 ms	6.1 min
0.3	7.2 ms	10 ms	9.9 s
0.1	270 μs	380 μs	370 ms
0.05	34 μs	48 μs	46 ms

[a] τ_c corresponds to a root mean square rotation of 1 rad.[13,30]

As is evident from the table, smaller particles rotate rapidly, allowing rapid observation of rotation. Decreasing the particle size from the 13 μm particle originally used by Perrin to a 130 nm particle, decreases rotation time, in the same fluid viscosity, by a factor of 1 million. Also, the smaller size allows one to study the local hydrodynamics for nanospheres embedded in micro- or nanoenvironments, i.e., the deviations from simple Brownian behavior in systems that exhibit hindered rotational motions, which may characterize an interface, pore, micelle, or biological cellular compartment.[7−9,11,13,31,32]

Experimental Method

MOONs can be prepared by coating one hemisphere of a particle with an opaque metal so that light is emitted only from the other hemisphere (moon-shaped particles).[1,33] A second type of MOON, aspherical MOONs, have aspherical shapes and emit different fluxes (and/or polarizations) of light from different geometric faces due to absorption and total internal reflection within the particle.[2,34,35] Here, we focus mainly on metal-capped MOONs.

Numerous methods are available to prepare microspheres and nanospheres. Inverse micelle polymerization[36] is employed to produce microspheres from a variety of polymer materials. Other preparation methods include Stober synthesis for silica nanoparticles[37] and grinding larger polymer blocks into microscopic particles with a mortar and pestle.[38] Nanoparticles can be further modified by chemically functionalizing their surfaces, "breading" them with fluorescent or magnetic nanocrumbs,[2,34] swelling them with dyes and ionophores,[39] and/or metal capping to form MOONs.[1]

The Brownian MOONs described in this text were prepared using commercially available microspheres and nanospheres. Fluorescent polystyrene spheres 850 nm in diameter were purchased from Spherotech (Libertyville, IL). Fluorescent polystyrene spheres 170 nm to 3.4 μm in diameter were obtained from Bangs Labs (Fishers, IN). A typical preparation method to make metal-capped Brownian MOONs using these fluorescent particles is illustrated in Figure 1 and described as follows:

(i) We deposit a monolayer of microspheres or nanospheres containing fluorescent material onto a glass microscope slide: This is accomplished by dispersing the microspheres/nanospheres in water or ethanol solution and spreading a drop of solution onto a glass slide and letting it dry. After the particles

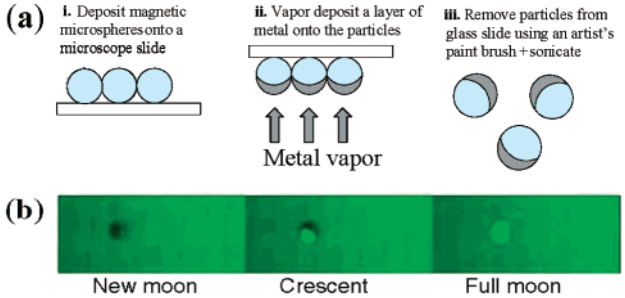

Figure 1. (a) Preparation of metal-capped modulated optical nanoprobes by vapor deposition. (b) Images of Brownian MOONs prepared by vacuum metalization. The fluorescent nanoprobes are shown in different orientations with a constant fluorescent background.

have dried the slide is examined under a microscope to confirm sufficient coverage and single-layer thickness.

(ii) Next, the microscope slide is placed in either an aluminum vapor coater or a gold sputter coater. Aluminum vapor deposition is performed in a vacuum, so the vaporized aluminum moves in a straight line (conservation of momentum) from the source to the target, thereby coating only one hemisphere of the particles and leaving the other hemisphere in shadow. This results in consistent coating of the particles, with metal on the same face relative to the glass slide and to each particle.

(iii) The MOONs keep very well on the metal-coated glass slide. They can be removed from the slide at any point using an artist's paintbrush. Sonicating the brush at 42 kHz for 20 s in aqueous solution suspends the particles.

Metal-capped MagMOONs can be prepared similarly except magnetizable particles are deposited on the glass slide and magnetized prior to metal coating. MagMOONs respond to external magnetic fields allowing for fine control over their orientation and consequently emission. To modulate MagMOONs, a permanent magnet is held above the microscope stage and rotated with a stepper motor attached to the magnet. A program written in LABVIEW (National Instruments, Austin, TX) controls the stepper motor with pulses sent through the parallel port.

Brownian MOONs were suspended in glycerol water solutions with different viscosities and put into a demountable 100 mm quartz sample chamber (Starna, Atascadero, CA) The small thickness of this cell prevented convection from affecting the particle motion. Brownian MOONs were viewed with an Olympus IMT-II (Lake Success, NY) inverted fluorescence microscope. Particles were viewed at low magnification, 4× and 10× objectives, to minimize bleaching and blinking resulting from movement in and out of the focal plane. Fluorescence spectra were acquired using an Acton Research Corp. spectrograph and a Hamamatsu HC230 CCD interfaced with an Intel Pentium computer. Images and videos of Brownian MOONs were acquired with a Nikon Coolpix 995 digital camera or a Photometrics Coolsnap ES CCD camera from Roper Scientific. The maximum acquisition rate for the Coolsnap CCD is 15 ms per frame. This acquisition rate and readout plus shot noise limit the angular resolution of analysis for Brownian MOONs. For larger particles the angle can be determined by the shape of the crescent. This is limited by magnification and fluorescence intensity from the MOON.

A series of images of MOONs were acquired using MetaMorph software from Universal Imaging Corporation. The resulting image stacks, consisting of from 1500 to 20 000 images, were analyzed to extract the blinking time series of Brownian MOONs undergoing rotational diffusion. Analysis of

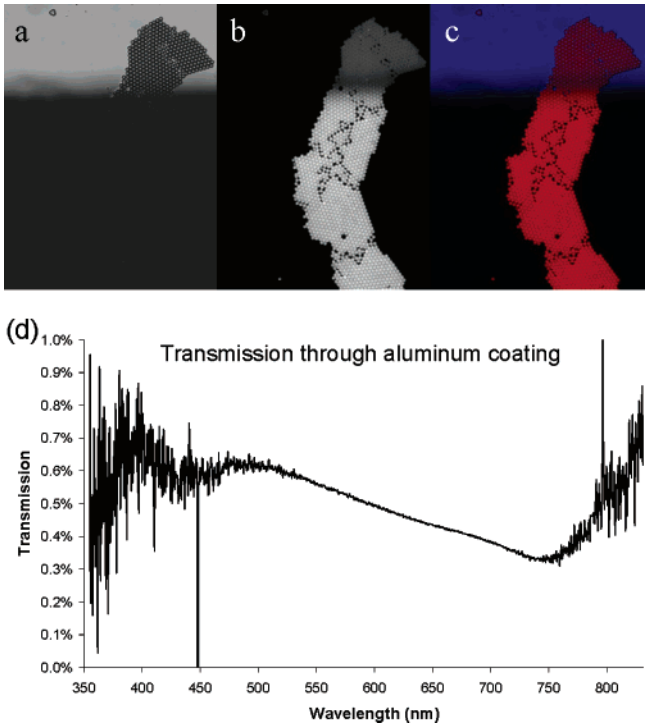

Figure 2. A monolayer aggregate of 3.4 μm microspheres with aluminum coating on the bottom $^3/_4$ of the view. (a) Bright field image at the edge of the metal coating with high transmission on the top where the metal coating is absent. (b) Fluorescence from coated particles (bottom) and uncoated particles (top). The metal coating results in higher intensity fluorescence. (c) Overlaid bright field and fluorescence image. (d) Transmission spectrum through the aluminum layer. The noise at high and low wavelengths is due to low signal from an incandescent lamp source. The coating thickness is estimated to be 50 nm.

the time series was performed with Matlab V. R13 from Mathworks, using vendor-supplied and locally written scripts.

A range of glycerol (spectroscopic grade, Sigma) water mixtures were prepared by percent weight, using a Mettler-Toledo analytical balance. Glycerol concentrations ranged from 0% to 95% glycerol by mass. The solutions were stored in sealed containers to prevent absorption of water.

Rat macrophages were cultured in Dulbecco's modified Eagle medium. Five days prior to nanosensor delivery and testing, the cells were removed from the culture dishes using trypsin and plated on uncoated 22 mm glass coverslips. Twenty-four hours before observations were made, a 50 μL aliquot of Brownian MOONs in 10 mM phosphate-buffered saline was added to the culture media for each cover slip.

Results and Discussion

The optical and physical characteristics of the MOONs were determined before and after removal from the glass slide. The thickness of metal capping deposited on the MOONs is determined by using a piezoelectric thickness monitor during the vacuum deposition process. It can then be verified by measuring the percentage of light transmitted through the metal coating compared to an uncoated portion of the slide (Figure 2a), assuming a skin depth of 9 nm for aluminum and 17 nm for gold for light of wavelength 589 nm.[40] Interestingly, the metal capping increases the fluorescence intensity emitted from capped microspheres. This is illustrated in parts b and c of Figure 2, where particles oriented toward the objective emit approximately 2.3 times more light than the adjacent uncapped microspheres. This enhancement may arise from increased

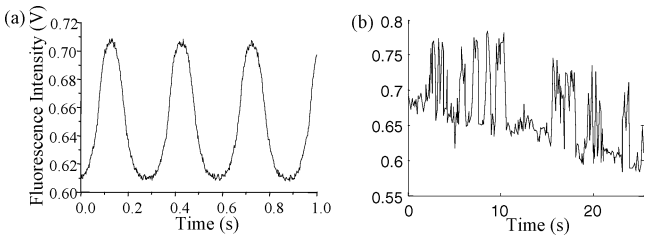

Figure 3. (a) Sinusoidal modulation of fluorescence intensity mediated by external magnetic control of MagMOON orientation. (b) In the absence of an external magnetic field, or if a MOON contains no magnetic material, the probe is modulated randomly solely due to Brownian rotation.

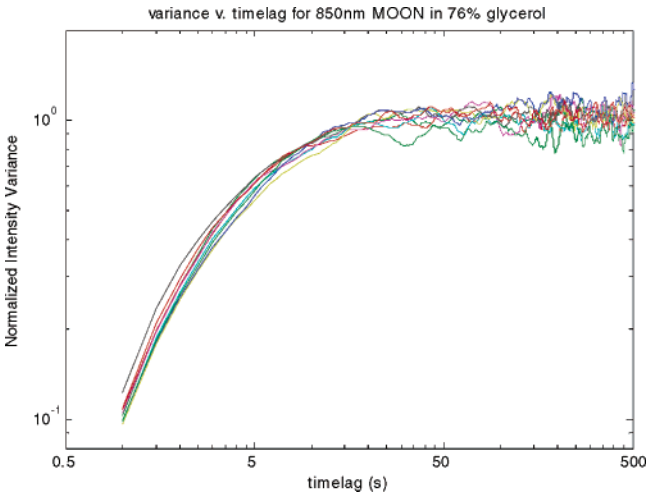

Figure 4. The mean square intensity fluctuation (angular displacement) for nine 850 nm Brownian MOONs rotating simultaneously in a 76% glycerol solution at 24 °C. Note the log−log scale. The analysis used 4000 images, acquired with a 500 ms delay between images.

excitation path length as well as reflection toward the objective of fluorescence that would usually be emitted away from the objective. Near-field and plasmon effects may also play a role, especially for smaller particles.

The intensity emitted from a MagMOON as a function of its orientation is determined by using a magnet to control the rotation of the MOON. The resulting periodic intensity waveform, shown in Figure 3a, has a fundamental frequency as well as a first harmonic of approximately $^1/_3$ the magnitude and some weaker higher order harmonics.[1] In the absence of external rotating magnetic fields, or for MOONs containing no magnetic material, the only surviving rotational motion of the nanoparticles or nanospheres is due to Brownian motion (rotation) as shown in Figure 3b. This time series of intensity fluctuations contains information about the particle shape, size, and its interaction with its environmental. Torques experienced by the particle and revealed by the blinking pattern include viscous drag, elastic forces, binding interactions, gravitational torques, vorticity in fluid flow, and biomechanical forces.

In the prepared glycerol water solutions, viscous drag is the only significant torque damping the Brownian MOON fluctuations. The rotational diffusion equation predicts that, for short times, the mean square angular displacement increases linearly with time (see eq 1). As a result of the periodic boundary conditions, at 0° and180°, the mean square angular displacement over a long time period exponentially approaches a maximum value. Experimentally, we calculate the mean square intensity fluctuation as $\langle \Delta I^2(\tau) \rangle = \langle [I(t + \tau) - I(t)]^2 \rangle$, as a function of time lag, τ. Figure 4 shows $\langle \Delta I^2(\tau) \rangle$ resulting from rotational diffusion of nine different 850 nm Brownian MOONs in a 76%

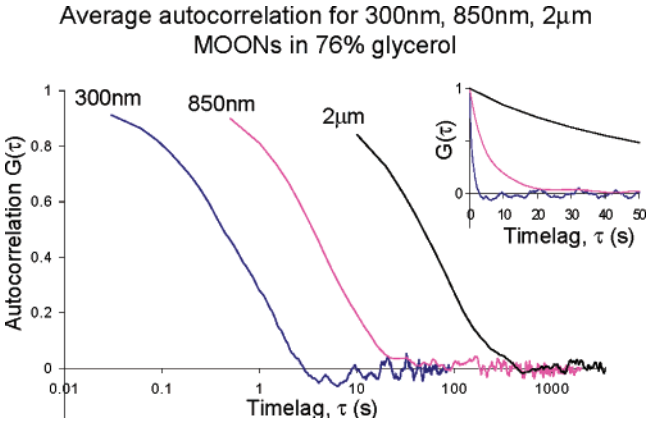

Figure 5. The autocorrelation functions for 300 nm, 850 nm, and 2 μm Brownian MOONs with a 50 nm aluminum coating in 76% glycerol solution at 24 °C. Inset: same data series plotted on linear axes.

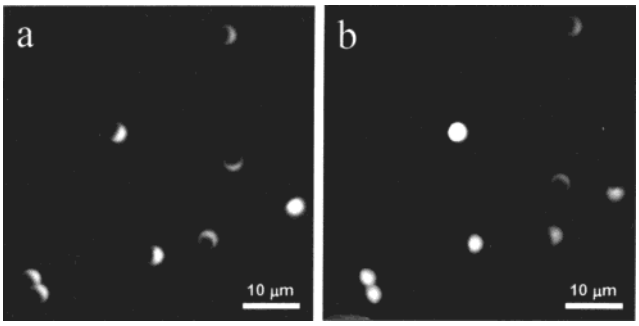

Figure 6. (a) Image of 3.4 μm Brownian MOONs in different orientations (phases of the moon). (b) Seconds later, the particles have reoriented due to Brownian forces.

glycerol solution from the same image time series. Particle to particle variation in $\langle \Delta I^2(\tau) \rangle$ is small and arises from the limited sampling time of the stochastic process. In addition, variations in particle size, angular intensity function, and particle environment also affect the autocorrelation function and should be measured over longer acquisition times.

The autocorrelation function also provides a measure of the angular diffusion rate. Figure 5 shows the mean autocorrelation function for several replicates of 300 nm, 850 nm, and 2 μm Brownian MOONs in a 76% glycerol solution. The plot, presented on a semilog scale, shows decays with well-separated time constants (time to decay to 1/e). The quantitative aspects of this figure will be discussed in a future paper.

At high magnification the shape of the crescent of MOONs that are larger than the diffraction limit allows their orientation to be tracked about two axes. A small number of chains of two or more particles are formed during the preparation. The orientation of these chains can be tracked around all three axes, allowing complete characterization of the particle orientation (Figure 6). Rotation around the dimer axis is observed to be approximately 2 times slower than for single MOONs, while rotation of the dimer axis is at an even slower rate. Gravity reduces the amount (degrees) that 2 and 3 μm dimers rotate in the z direction. The rigid chains are held together by the aluminum coating and can be dispersed with further sonication.

At high particle concentrations, we are able to observe occasional interactions between particles and thus study the resulting aggregates. These aggregates can be directly observed for particles larger than 1 μm and inferred from the intensity rates for all particle sizes. Figure 7a shows the intensity fluctuations for a single 2 μm particle rotating in glycerol solution (top) and slower fluctuations for a single brighter

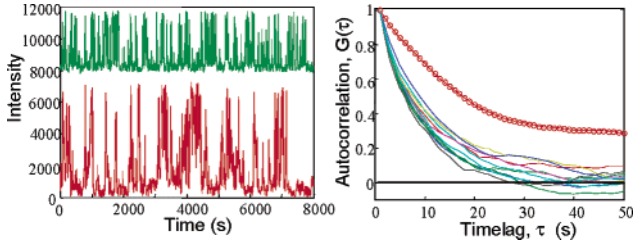

Figure 7. (a) The intensity time series for a single 850 nm polystyrene MOON (green) positively offset for comparison with a dimer (red). (b) The solid lines show typical autocorrelation functions of a time series for 10 single 850 nm Brownian MOONs with a 50 nm aluminum coating in 56% glycerol solution at 24 °C. Shown with circles is the autocorrelation function for a dimer of 850 nm MOONs from the same image series.

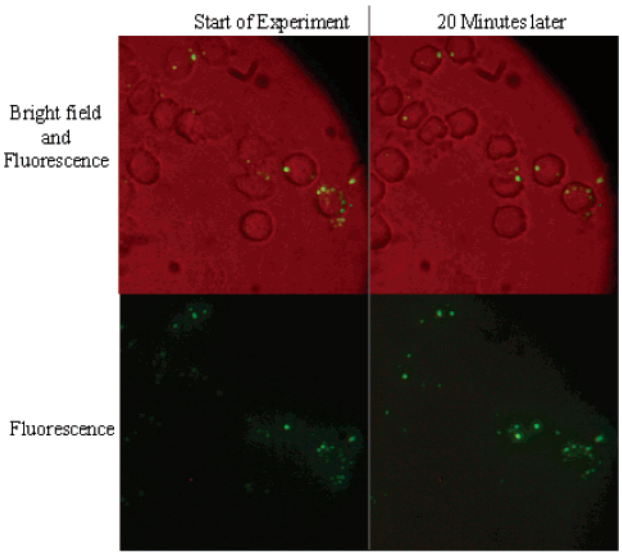

Figure 8. Brownian MOONs reorienting in macrophages. Top: overlaid bright field and fluorescence images showing Brownian MOONs internalized by rat macrophages at two different times, start of the experiment (left) and 20 min later (right). Bottom: Fluorescence images of Brownian MOONs reorienting in rat macrophages.

particle (an aggregate) rotating in the same image series (bottom). Figure 7b shows the autocorrelation function for the aggregate as well as for 10 single spherical 2 μm Brownian MOONs. The decay time for the aggregate is approximately twice the average decay time for the single particles.

In addition to studying particle interactions, Brownian MOONs can be used to probe environmental viscoelastic and biomechanical forces. On the microscopic scale, measurements of viscosity in the cell cytosol have varied over 6 orders of magnitude, depending on the size of the probe used.[12] Recent work suggests sievelike structures within subdomains of cytoplasm, which allow small particles to diffuse through while resisting the motion of larger particles.[41] In addition, liquid filled structures such as endosomes may allow particles to rotate within but not translate, causing divergence between rotational and translational Brownian diffusion. Figure 8 shows Brownian MOONs reorienting within macrophage endosomal compartments. This approach allows direct observation of endosome properties and torques on the endosome, on an individual particle and endosome basis. Combined with modulated chemical sensing,[36] this method is a tool for directly probing intracellular physiology and dynamics.

Interpretation of intensity time fluctuations is limited by the approximations used to describe the fluorescence intensity of the MOONs as a function of angle. Modeling this function is

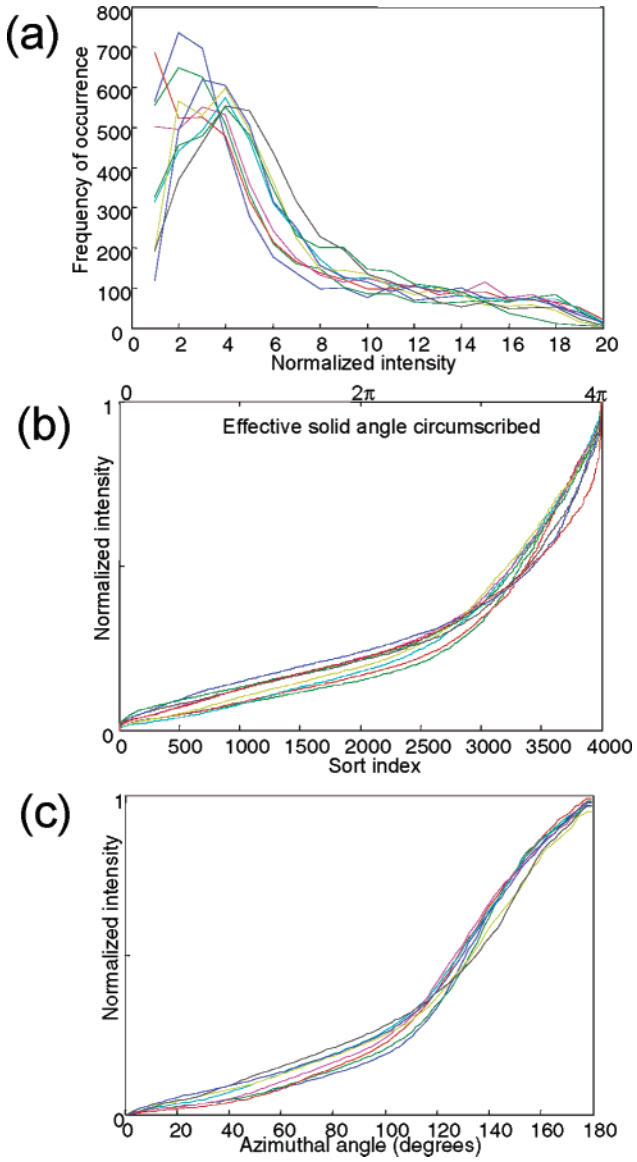

Figure 9. (a) Histogram showing the frequency of occurrence of each observed intensity for 850 nm particles in 76% glycerol solution. (b) Sorted intensity values for the same particles as a function of sort index or effective solid angle (see text). (c) Intensity is plotted vs azimuthal angle for the same particles.

difficult because it necessitates accounting for subwavelength scattering and absorption of excitation and emission wavelengths within the particle and from the metal capping. For instance, Figure 2 illustrates that the metal capping enhances the fluorescence from the 3.4 μm MOONs observed at full moon phase. Intensity angle fluctuations obtained from rotating 4.4 μm MagMOONs indicate that the MagMOON intensity increases monotonically with angle, that there is a first harmonic at about $^1/_3$ the amplitude of the driving magnetic field rotation, and that they spend more time in dark phases than in bright phases. Brownian MOONs, with different sizes, with no absorbing magnetic material, and with different fluorescent dyes, may have different angle intensity functions. In addition, particle shape and binding may also affect these functions.

Information about the angle intensity function is contained within the intensity time series. Figure 9a shows histograms of normalized intensities from a group of eight randomly orienting 850 nm MOONs. The histograms indicate that the MOONs emit low-intensity light more frequently than high-intensity light. Figure 9b shows the intensities from the same particles sorted

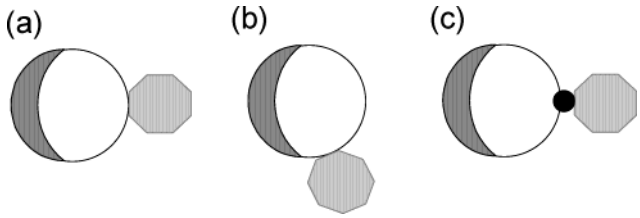

Figure 10. Cartoon representing a particle binding to a MOON. (a) and (b) show the particle binding to different locations on the MOON relative to the capping, creating different amounts of drag around the azimuthal axis. (c) Using local breading to control the location of the binding target.

from lowest intensity to highest intensity. Assuming that the MOON is symmetrically capped, that the MOON brightness increases monotonically with azimuthal angle, and that each MOON samples all orientation states with equal probability, this sorted intensity plot is equivalent to a plot of intensity versus solid angle. This plot can be transformed into an intensity versus azimuthal angle plot by taking into account that the number of states corresponding to each azimuthal angle is proportional to the sine of the azimuthal angle, just as the circumference of a sphere varies with latitude. The intensity angle functions for the eight 850 nm Brownian MOONs shown in Figure 9c are similar from particle to particle. These plots resemble the functions previously obtained using 4.4 μm MagMOONs, although they show more of a bias toward orientations in dark phases. This analysis can be used to characterize the angle intensity function from individual nanoprobes.

An unbound particle is expected to sample all orientation states with equal probability, except when influenced by external forces. Brownian MOONs are useful tools for exploring these torques; however, the effect from the constant force of gravity should be considered in such studies. In certain cases gravity can exert significant torques. Gravitational pull on a 1 μm MOON with a 100 nm thick gold cap produces a force on the cap of $\sim$14 fN. Assuming that the center of mass for a metal-capped MOON is located at about half of the radius from the sphere center, the result is an energy difference between up and down orientations of $\sim$1.7 kT at room temperature. This results in a 5:1 probability ratio for fully down to fully up orientation. The energy difference increases with the total volume and density of the capping material, as well as with particle radius (height). These effects are minimized by using thinner coatings, using substantially lower density metal capping materials such as aluminum, and by using smaller particles with less surface area and height. For a 2 μm MOON with 50 nm of aluminum there is an energy difference between the up and down states that results in a 2:1 probability ratio for fully down to fully up. The effect is negligible for smaller MOONs due to their smaller cap weights and reduced radius (height).

Conclusion

Tracking angular fluctuations allows sensitive measurements of torques acting on Brownian MOONs. This will enable high-resolution images of viscoelastic properties of local environments. It also allows characterization of the drag on a MOON induced by binding, such as the binding of 50 nm viruses to 100 nm Brownian MOONs. Some of these applications require control over binding location relative to the capping material because the location of the binding affects the rotation rate. Control could be achieved by chemically binding or physically pressing ("breading") smaller particles into large particles before metal capping,[2,34,42] as shown in Figure 10.

Controlling the optical symmetry of particles produces new tools for the exploration of optical, chemical, and materials properties of surrounding environments. They can be used as nanoinstruments such as nanoviscometers,[4,9,33,42−45] nanothermometers,[46] nanobarometers, and nanochemical sensors.[39,47−52] Modulation of Brownian MOONs and MagMOONs[1−3] also allows the local optical, chemical, and materials properties to be distinguished from the bulk properties. These novel tools promise intracellular chemical imaging with much improved signal over background, high sensitivity immunoassays with simpler procedures, measurements of viscosities at chosen time and size scales, observation of microvorticity in fluids, as well as simultaneous intracellular physical and chemical imaging.

Acknowledgment. The authors gratefully acknowledge Dr. Panos Argyrakis and Wei Yi for Monte Carlo simulations, Tom Horvath for his technical assistance, and support from NSF DMR-9900434 and DARPA F49620-03-1-0297.

References and Notes

(1) Anker, J. N.; Kopelman, R. *Appl. Phys. Lett.* **2003**, *82*, 1102−1104.
(2) Anker, J. N.; Behrend, C.; Kopelman, R. *J. Appl. Phys.* **2003**, *93*, 6698−6700.
(3) Behrend C. J.; Anker J. N.; Kopelman R. *Appl. Phys. Lett.* **2004**, *84*, 154−156.
(4) Anker, J. N.; Behrend, C. J.; McNaughton, B. H.; Roberts, T. G.; Brasuel, M.; Philbert, M. A.; Kopelman, R. *2004 Proc. Mater. Res. Soc.*, in press.
(5) Lakowicz, J. R. *Principles of Fluorescence Spectroscopy*; Plenum Press: New York, 1983.
(6) Lugowski, R.; Kolodziejczyk, B.; Kawata, Y. *Opt. Commun.* **2002**, *202*, 1−8.
(7) Crick, F. H. C.; Hughes, A. F. W. The Physical Properties of Cytoplasm: a Study by Means of the Magnetic Particle Method. *Exp. Cell. Res.* **1950**, *37*, 80.
(8) Gisler, T.; Weitz, D. A. *Curr. Opin. Colloid Interface Sci.* **1998**, *3*, 586−592.
(9) Mackintosh, F. C.; Schmidt, C. F. *Curr. Opin. Colloid Interface Sci.* **1999**, *4*, 300−307.
(10) Mason, T. G.; Weitz, D. A. *Phys. Rev. Lett.* **1995**, *74*, 1250−1253.
(11) Koenderink, G. H. *Rotational and Translational Diffusion in Colloidal Mixtures*; Cip-Gegevens Koninklikjke Bibliotheek: Dan Haag, The Netherlands, 2003.
(12) Valberg, P. A.; Feldman, H. A. *Biophys. J.* **1987**, *52*, 551−561.
(13) Valberg, P. A.; Butler, J. P. *Biophys. J.* **1987**, *52*, 537−550.
(14) Moller, W.; Hofer, T.; Ziesenis, A.; Karg, E.; Heyder, J. *Toxicol. Appl. Pharmacol.* **2002**, *182*, 197−207.
(15) Romano, G.; Sacconi, L.; Capitanio, M.; Pavone, F. S. *Opt. Commun.* **2003**, *215*, 323−331.
(16) Perrin, J. *Brownian Movement and Molecular Reality*; Taylor and Francis: London, 1910.
(17) Tsuda, Y.; Yasutake, H.; Ishijima, A.; Yanagida, T. *Proc. Natl. Acad. Sci. U.S.A.* **1996**, *93*, 12937−12942.
(18) Yasuda, R.; Miyata, H.; Kinosita, K. *J. Mol. Biol.* **1996**, *263*, 227−236.
(19) Cheng, Z.; Mason, T. G. *Phys. Rev. Lett.* **2003**, *90*, 01804-1−01804-4.
(20) Takei, H.; Shimizu, N. *Langmuir* **1997**, *13*, 1865−1868.
(21) Nakahama, K.; Kawaguchi, H.; Fujimoto, K. *Langmuir* **2000**, *16*, 7882−7886.
(22) Himmelhaus, M.; Takei, H. *Sens. Actuators, B* **2000**, *63*, 24−30.
(23) Fujimoto, K.; Nakahama, K.; Shidara, M.; Kawaguchi, H. *Langmuir* **1999**, *15*, 4630−4635.
(24) Cameron, L. A.; Footer, M. J.; Van Oudenaarden, A.; Theriot, J. A. *Proc. Natl. Acad. Sci. U.S.A.* **1999**, *96*, 4908−4913.
(25) Lu, Y.; Xiong, H.; Jiang, X. C.; Xia, Y. N.; Prentiss, M.; Whitesides, G. M. *J. Am. Chem. Soc.* **2003**, *125*, 12724−12725.
(26) Crowley, J. M.; Sheridon, N. K.; Romano, L. *J. Electrost.* **2002**, *55*, 247−259.
(27) Choi, J.; Zhao, Y. H.; Zhang, D. Y.; Chien, S.; Lo, Y. H. *Nano Lett.* **2003**, *3*, 995−1000.
(28) Brown, R. *Edinburgh J. Sci.* **1829**, *1*, 314−319.
(29) Brown, R. *Edinburgh Philos. J.* **1828**, *5*, 358−371.
(30) Einstein, A. *Investigations on the Theory of the Brownian Movement*; Dover: New York, 1956.

(31) Tomishige, M.; Sako, Y.; Kusumi, A. *J. Cell Biol.* **1998**, *142*, 989−1000.
(32) Luby-Phelps, K. *Int. Rev. Cytol.* **2000**, *192*, 189−221.
(33) Anker, J. N.; Behrend, C.; Kopelman, R. Unpublished.
(34) Anker, J. N.; Horvath, T. D.; Kopelman, R. *Eur. Cells Mater.* **2002**, *3*, 95.
(35) Wang, J. F.; Gudiksen, M. S.; Duan, X. F.; Cui, Y.; Lieber, C. M. *Science* **2001**, *293*, 1455−1457.
(36) Clark, H. A.; Hoyer, M.; Philbert, M. A.; Kopelman, R. *Anal. Chem.* **1999**, *71*, 4831−4836.
(37) Xu, H. Ph.D. Thesis, University of Michigan, Ann Arbor, MI, 2003.
(38) Sasaki, K.; Shi, Z. Y.; Kopelman, R.; Masuhara, H. *Chem. Lett.* **1996**, 141−142.
(39) Brasuel, M.; Kopelman, R.; Miller, T. J.; Tjalkens, R.; Philbert, M. A. *Anal. Chem.* **2001**, *73*, 2221−2228.
(40) Born, M.; Wolf, E. *Principles of Optics*, 6th ed.; Cambridge University Press: New York, 1980; Chapter 13.
(41) Janson, L. W.; Ragsdale, K.; Lubyphelps, K. *Biophys. J.* **1996**, *71*, 1228−1234.
(42) Santhanam, V.; Andres, R. P. *Nano Lett.* **2004**, *4*, 41−44.
(43) Nicolas, Y.; Paques, M.; Knaebel, A.; Steyer, A.; Munch, J. P.; Blijdenstein, T. B. J.; Van Aken, G. A. *Rev. Sci. Instrum.* **2003**, *74*, 3838−3844.
(44) Breedveld, V.; Pine, D. J. *J. Mater. Sci.* **2003**, *38*, 4461−4470.
(45) Van Vliet, K. J.; Bao, G.; Suresh, S. *Acta Mater.* **2003**, *51*, 5881−5905.
(46) Zohar, O.; Ikeda, M.; Shinagawa, H.; Inoue, H.; Nakamura, H.; Elbaum, D.; Alkon, D. L.; Yoshioka, T. *Biophys. J.* **1998**, *74*, 82−89.
(47) Monson, E.; Brasuel, M.; Philbert, M. A.; Kopelman, R. *Biomedical Photonics Handbook*; CRC Press: Boca Raton, FL, 2003.
(48) Xu, H.; Yan, F.; Monson, E. E.; Kopelman, R. *J. Biomed. Mater. Res. Part A* **2003**, *66A*, 870−879.
(49) Clark, H. A.; Hoyer, M.; Parus, S.; Philbert, M. A.; Kopelman, M. *Mikrochim. Acta* **1999**, *131*, 121−128.
(50) Xu, H.; Aylott, J. W.; Kopelman, R. *Analyst* **2002**, *127*, 1471−1477.
(51) Aylott, J. W. *Analyst* **2003**, *128*, 309−312.
(52) Xu, H.; Aylott, J. W.; Kopelman, R.; Miller, T. J.; Philbert, M. A. *Anal. Chem.* **2001**, *73*, 4124−4133.